Nano Research 2017, 10(9): 3077–3091
DOI 10.1007/s12274-017-1523-5
Research Article
ISSN 1998-0124
CN 11-5974/O4

Curved copper nanowires-based robust flexible transparent electrodes via all-solution approach

Zhenxing Yin[1,§], Seung Keun Song[2,§], Sanghun Cho[1], Duck-Jae You[1], Jeeyoung Yoo[1], Suk Tai Chang[2] (✉), and Youn Sang Kim[1,3] (✉)

[1] *Program in Nano Science and Technology, Graduate School of Convergence Science and Technology, Seoul National University, Seoul 08826, Republic of Korea*
[2] *School of Chemical Engineering and Materials Science, Chung-Ang University, Seoul 06974, Republic of Korea*
[3] *Advanced Institutes of Convergence Technology, 145 Gwanggyo-ro, Yeongtong-gu, Suwon-si, Gyeonggi-do 16229, Republic of Korea*
[§] *Zhenxing Yin and Seung Keun Song contributed equally to this work.*

Received: 4 January 2017
Revised: 5 February 2017
Accepted: 9 February 2017

KEYWORDS
curved Cu nanowires,
all-solution processes,
20 μm patterns,
high performance,
transparent electrode

ABSTRACT

Curved Cu nanowire (CCN)-based high-performance flexible transparent conductive electrodes (FTCEs) were fabricated via a fully solution-processed approach, involving synthesis, coating, patterning, welding, and transfer. Each step involved an innovative technique for completing the all-solution processes. The high-quality and well-dispersed CCNs were synthesized using a multi-polyol method through the synergistic effect of specific polyol reduction. To precisely control the optoelectrical properties of the FTCEs, the CCNs were uniformly coated on a polyimide (PI) substrate via a simple meniscus-dragging deposition method by tuning several coating parameters. We also employed a polyurethane (PU)-stamped patterning method to effectively produce 20 μm patterns on CCN thin films. The CCN thin films exhibited high electrical performance, which is attributed to the deeply percolated CCN network formed via a solvent-dipped welding method. Finally, the CCN thin films on the PI substrate were partially embedded and transferred to the PU matrix to reduce their surface roughness. Through consecutive processes involving the proposed methods, a highly percolated CCN thin film on the PU matrix exhibited high optoelectrical performance (R_s = 53.48 Ω/□ at T = 85.71%), excellent mechanical properties (R/R_0 < 1.10 after the 10th repetition of tape peeling or 1,000 bending cycles), and a low root-mean-square surface roughness (R_{rms} = 14.36 nm).

1 Introduction

Metal nanowire (NW)-based flexible transparent conductive electrodes (FTCEs) have attracted considerable attention owing to their demand in flexible electronics [1, 2]. To date, most transparent electrodes in modern

Address correspondence to Youn Sang Kim, younskim@snu.ac.kr; Suk Tai Chang, stchang@cau.ac.kr

flat-panel electronics are made with indium tin oxide (ITO) materials owing to their good electrical conductivity and high transparency in the visible range [1, 3]. However, the scarcity of In and the high-vacuum sputtering required for manufacturing make the cost too high for the public [1, 4, 5]. More importantly, the high brittleness of ITO is a critical limitation that has prompted efforts to develop new alternatives for advanced flexible devices. In the past several years, solution-processable single-walled carbon nanotube (SWCNT) and reduced graphene oxide (RGO) thin films pioneered the development of FTCEs as substitute materials [6, 7]. Although FTCEs exhibit excellent conductivity and remarkable flexibility, the high contact resistance at their junctions is an obstacle for high electrical performance [6, 8]. SWCNTs and RGO are particularly useful for the development of useful devices, such as sensors, supercapacitors, and batteries [9–11]. However, entirely replacing ITO with these materials for flexible optical devices is difficult.

As the most promising materials for replacing ITO, solution-processable Ag and Cu NW thin films have been extensively explored for FTCEs because of their low sheet resistance, high transparency, and outstanding flexibility [12, 13]. To fabricate FTCEs from these materials, metal NWs are randomly distributed on the transparent substrate via a solution-based coating method and deeply percolated within its networks via thermal welding. The large areas produced by uncovered NW films ensure a high transparency. The connected NW networks provide electron transference, yielding excellent electrical conductivity. Furthermore, the inherent metallic ductility and high aspect ratio of the one-dimensional NW structure are beneficial for the flexibility of FTCEs. Although many reported Ag and Cu NW thin films have superior functional properties to ITO, their high surface roughness and difficulty of patterning limit their applications in FTCEs for flexible devices [14, 15]. Moreover, the high cost of material synthesis must be reduced for widespread commercialization. In particular, Ag NW thin films have been comprehensively researched, exhibiting considerable optoelectrical performance [12, 16]. However, Ag is a noble metal that has been even more expensive and scarce than In in recent years [17].

Compared with Ag, Cu-based materials are abundant, significantly cheaper, and have nearly identical electrical properties, making them suitable for the requirements of the electronics market [18]. In our previous study, we synthesized Cu NWs with curved structures using a low-cost and simple binary polyol method and coated them on a polyethylene terephthalate (PET) substrate as an FTCE [19]. The curved Cu NWs (CCNs) not only provided shape control but also enhanced the mechanical properties of the FTCEs, as the self-bendable structure induced good ductility and softness [19]. Compared with straight nanowires, CCNs usually occupy more space and have the same electron-transfer properties; thus, they more easily form an effective network. Furthermore, the curved shape has a smaller point-to-point linear distance per NW, resulting in higher optoelectrical performance and patternability for FTCEs [19]. However, several technical issues must be solved for the practical applications of CCNs, such as their low robustness, high surface roughness, and difficulty of patterning. Additionally, few Cu NW-based FTCEs have been fabricated via all-solution processes without complicated material synthesis, expensive facilities, or harsh conditions.

Herein, we propose an all-solution approach for the entire manufacturing process of CCN-based FTCEs, comprising multi-polyol synthesis, meniscus-dragging deposition (MDD), polyurethane (PU)-stamped patterning, solvent-dipped welding, and PU-embedded transfer. Furthermore, a series of innovative methods are suggested for solving the technical issues regarding the fabrication of CCN-based FTCEs with high optoelectrical performance, such as the low robustness, high surface roughness, and difficulty of patterning.

2 Experimental

2.1 Preparation of CCNs via multi-polyol synthesis

In a typical synthesis procedure, 2 mmol of a CuCl precursor, 6 mmol of an oleylamine surfactant, and 0.3 mmol of an ammonium-chloride surfactant were dissolved in a reductant containing the following mixed polyols: 15 mL of ethylene glycol (EG), 10 mL of glycerol (GC), and 5 mL of polyethylene glycol$_{200}$ (PEG_{200}). The Cu^{+}-amine complex was fully formed

via strong magnetic stirring when the reaction temperature was increased to 110 ℃. After 15 min, the temperature was increased to 208 ℃ at a heating rate of 9 ℃/min, followed by 20 min of refluxing. The resulting red-brown CCNs, which were completely prepared, were cooled to 25 ℃ via cold-water quenching. The CCNs were washed with n-hexane and ethanol and centrifuged for 5 min at 6,000 rpm. The washing and centrifugation were repeated three times. Finally, the CCNs were re-dispersed in cyclohexane for the coating step.

2.2 CCN film coating via MDD

An ethanol-washed polyimide (PI) film and a slide glass were prepared as the coating substrate and deposition plate, respectively. We injected 20 μL of a CCN dispersion (1.5 mg/mL) between the prepared PI substrate and the deposition plate using a micropipette at a deposition angle of θ = 30°. The trapped CCN meniscus was spread ten times on the coating plate via linear back- and-forth motion at a speed of 40 mm/s. After the solvent of the CCN film was dried, a specific number of additional CCN coatings was applied on the CCN film, yielding an aligned CCN film. The substrate with the aligned CCN film was rotated by 90°, and CCNs were vertically deposited on the parallel CCN film using the same method. After repeating these procedures, we obtained a crossed-formation CCN film on the imide substrate.

2.3 CCN film patterning via PU-stamped patterning

Two parts of a urethane liquid compound (Clear Flex® 95, Smooth-On) were mixed at a weight ratio of 1.5:1 and pre-cured on a line-space patterned polydimethylsiloxane (PDMS) mold at a constant temperature of 40 ℃. After 5 h of pre-curing, the reverse-patterned PU matrix was obtained. The pre-cured PU matrix was directly stamped onto the CCN thin film (77.26% T of sample, before washing) for 1 h with 0.12 N/cm^2 of pressure. The CCNs were completely embedded in the convex parts of the PU matrix, which was carefully peeled from the PI substrate.

2.4 CCN percolation via solvent-dipped welding

The CCN thin film on the PI substrate was covered by a PEG_{200} solvent. When the temperature was increased to 200 ℃ for 30 min, the natural oxide layer was sufficiently reduced, and the film gradually became conductive. A pressure of 0.3 N/cm^2 was applied on the CCN thin film using a weight, while the other conditions were kept unchanged. After another 30 min of pressing for complete percolation, the weight was carefully removed from CCN thin film. The CCN thin film was rapidly placed in acetone, and the temperature of the PEG_{200} was reduced to 140 ℃. Finally, the CCN thin film was washed with acetone to remove the residual PEG_{200}.

2.5 CCN film smoothing via PU-embedded transfer

Two parts of the urethane liquid compound (Clear Flex® 95, Smooth-On) were mixed at a weight ratio of 1.5:1 and pre-cured on a flexible transparent substrate (PET, PDMS) at a constant temperature of 40 ℃. After 10 h of pre-curing, the PU matrix was kept in contact with the CCN thin film for 30 min with an applied pressure of 0.3 N/cm^2. Then, the CCNs were successfully transferred to the PU matrix when it was carefully peeled from the PI substrate. The PU matrix was completely cured through an additional 2 h of curing at 40 ℃. The flexible transparent substrate was easily peeled from the PU matrix if required.

2.6 Characterization of CCNs and FTCEs

The prepared CCNs were characterized using scanning electron microscopy (SEM, Hitachi S-4800 FE-SEM), X-ray diffraction measurements (Bruker D8 DISCOVER), ultraviolet–visible (UV–vis) spectroscopy (PerkinElmer Lambda 35), and high-resolution transmission electron microscopy (HR-TEM, JEOL JEM-2100F). The optoelectrical performance of the CCN thin films was investigated using optical microscopy (OM, Olympus utv1x-2), UV–vis–near-infrared spectrophotometry (Jasco V-670), and a four-point probe (Keithley 2612A sourcemeter). The transmittance of the CCN thin films was calculated based on identical reference substrates, such as PI, PU, and PU/PET. Therefore, the transmittances proposed in this work were only measured for the CCN thin films, without considering the substrates. The surface roughness was measured using atomic-force microscopy (AFM, Park Systems XE-100).

3 Results and discussion

3.1 Synthesis process

The CCN-based smooth, robust, and patternable FTCEs were fabricated by a combination of several innovative techniques—as illustrated in Scheme 1 and Fig. S1 in the Electronic Supplementary Material (ESM)—including synthesis, coating, patterning, welding, and transfer. Although many researchers emphasize the low price of Cu NWs, the use of expensive reagents, catalysts, and instruments, as well as the experimental conditions, make FTCEs with Cu NWs even more expensive to fabricate than those with Ag NWs [20, 21]. To overcome this problem, the CCNs were prepared with a commonly used reagent in a short reaction time of 1 h via a multi-polyol synthesis method and homogeneously dispersed in a cyclohexane solvent, which was modified from the binary polyol system, for the coating step [19]. The multi-polyol synthesis method used in this study solved the problems of low purity and CCN aggregation that we previously encountered.

The shape of the Cu NWs was clearly changed by controlling the reduction solvent types and ratio, as shown in Figs. S2–S4 in the ESM. With a single polyol, the precursors experienced the same reduction conditions, resulting in the atomic arrangement of symmetrical decahedron-shaped seeds with the effect of the salt ions, and grew in the [1$\bar{1}$0] direction, forming linear Cu NWs [22–24]. The dimensions of the Cu NWs clearly differed depending on the polyol types, because of the different reduction potentials arising from the variations in their molecular structures (Fig. S2 in the ESM). From the SEM images, we infer that the polyol reducing ability at 198 °C decreased in the following order: GC > EG > diethylene glycol > PEG_{200}. To observe the relevance of the Cu NW morphology and the co-reduction effect, various binary polyol systems were investigated, as shown in Fig. S3 in the ESM. The GC/EG mixture was the only suitable synthesis condition for the CCNs. As previously reported, EG and GC reduce Cu^{+}-amine ions, forming asymmetric decahedral multiply twin particles via the co-reduction effect and reduction-potential gap. Thus, they grow in the [1$\bar{1}$0] direction of curved structural NWs with plastic deformation due to partial line defects [19, 25, 26]. However, the low purity arising from the curved shape and the CCN aggregation are

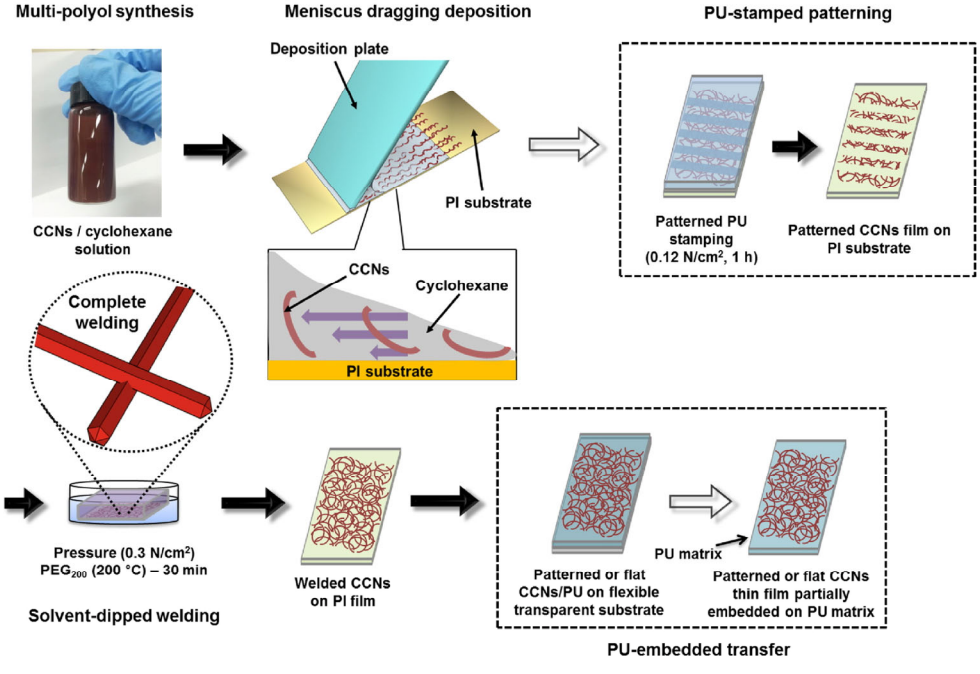

Scheme 1 Fabrication of the smooth, robust, and patternable CCN-based FTCEs via all-solution processes, including synthesis, coating, patterning, welding, and transfer. In the MDD, the flow speed of the upper layer was higher than that of the lower layer. This flow-speed difference (indicated by parallel arrows in solvent) caused the wires to form an orderly arrangement on the substrate.

problems that must be addressed for the homogeneous distribution of CCNs in the coating process. Normally, the active peripheral atoms, large surface area, and curved structure of CCNs yield a high surface energy [19, 27]. To reach a steady state, a passivation layer is usually formed on the CCN surface via reactions with negative elements and the adsorption of surfactants [22, 28]. Nevertheless, the dominant reduction condition and high reaction temperature in the synthesis process restrain the surface passivation, resulting in the easy aggregation of CCNs. In this study, we added PEG_{200} to the EG/GC mixtures to significantly reduce the surface energy of the CCNs and prevented aggregation by controlling the CCN dimensions. Furthermore, the partially mild reduction condition due to the PEG_{200} altered the asymmetric degree of Cu seeds, enhancing the purity of the CCNs. Figure S4 in the ESM clearly shows the morphological changes arising from different mixing ratios of GC, EG and PEG_{200}. In the optimal condition of 15 mL of EG, 10 mL of GC, and 5 mL of PEG_{200}, the PEG_{200} was well blended with the GC and EG, which allowed the easy preparation of multiple highly asymmetric decahedral Cu seeds, yielding high-purity CCNs with good curvature. However, with excessive amounts of PEG_{200}, the CCNs lost their curved structure because the mild reductant PEG_{200} was dominant in the ternary polyol system, reducing the asymmetry of the Cu seeds. Figure 1 shows SEM images and XRD spectra of the synthesized CCNs. In the SEM images, an average width of 65 nm and length of 25 μm were measured for dozens of randomly selected, highly curved Cu NWs (Figs. 1(a)–1(c)). In the XRD patterns of the CCNs (Fig. 1(d)), the three characteristic peaks at 2θ = 43.5°, 50.7°, and 74.4° are assigned to the typical {111}, {200}, and {220} planes, respectively, of face-centered cubic Cu (JCPDS #03-1018), indicating a pure phase. The absorption peak of the CCNs was located at 573 nm, owing to the surface plasma resonance caused by the oscillation of free electrons in the conduction band (Fig. S5 in the ESM).

3.2 Coating process

After the synthesis process, the CCNs were preserved and well dispersed in cyclohexane, as shown in Scheme 1. Generally, the dispersion of NWs is strongly related to the compatibility, polarity, and viscosity of the dispersible solvent [29]. Although cyclohexane has a weak polarity, its viscosity is more than three

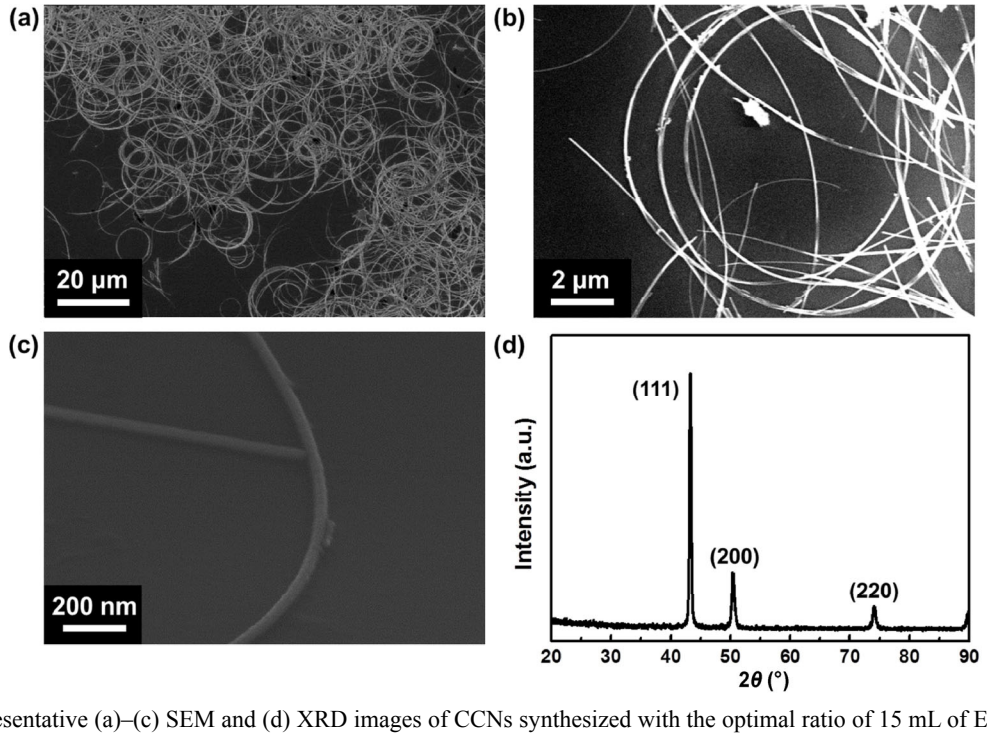

Figure 1 Representative (a)–(c) SEM and (d) XRD images of CCNs synthesized with the optimal ratio of 15 mL of EG, 10 mL of GC, and 5 mL of PEG_{200}.

times that of n-hexane. This is attributed to the ring structure of the molecule, which causes CCNs to be well dispersed. More importantly, the alkyl chains in cyclohexane induce a high hydrophobicity, which is compatible with oleylamine-capped CCNs deposited on a PI film. Moreover, the high vapor pressure of the solvent is suitable for solvent-volatilization coating methods, such as spin coating, wire-wound coating, spray coating, dip coating, convective assembly, and MDD. However, when applied over a large area, spin coating and wire-wound coating place limitations on the uniformity and efficiency of alignment. Furthermore, dip coating, spray coating, and convective assembly involve large consumption of materials and extremely long operation times. Therefore, we proposed a simple MDD method for the uniform, rapid, cost-effective, and large-area coating of CCNs on the PI substrate. The detailed process characteristics are shown in Table S1 in the ESM [30–37]. The commercial PI film is typically applied to actual devices via the roll-to-roll process because of its high glass transition temperature and outstanding flexibility.

When the CCNs/cyclohexane dispersion was injected between the PI substrate and the deposition plate, a meniscus of dispersion was quickly formed by the capillary action of the cyclohexane. The linear back-and-forth motion of the deposition plate dragged the liquid meniscus onto the PI substrate, and the CCNs were efficiently aligned through the shear gradient of fluid [30, 38], as shown in the coating process depicted in Scheme 1. Because the shear gradient of fluid was due to the linear motion of the deposition plate, we selected 40 mm/s as the optimal coating speed for the efficient alignment of the CCN thin film. Furthermore, the aspect ratio of the NWs is an important factor for efficient coating. When the CCN length exceeds 20 μm, the CCNs are arranged on PI substrate in an orderly manner, parallel to the dragging direction, because NWs with a high aspect ratio are more likely to be significantly influenced by the shear gradient of fluid. The solvent properties also contributed to the uniformity of the films. Because cyclohexane has the novel properties of a high volatility, low surface tension, and low viscosity, the solvent was quickly evaporated before disrupting the CCN alignment via Brownian motion. For this reason, the CCNs/cyclohexane dispersion can be easily applied for the MDD method to form a complete CCN network with any substrate, such as PET, glass, silicon wafers, or PI. In addition, the solvent-receding flow that occurred during the evaporation had little impact on the CCN alignment, owing to the pinning force acting on the CCNs at the edge of the liquid film [38]. Therefore, the film size was easily controlled by changing the width of the deposition plate, as shown in Fig. 2(a). To acquire the parameters related to the film-thickness control, it is important to consider the bond number (Bo) and capillary number (Ca). According to previous research, these are calculated using the following equations

$$\mathrm{Bo} = \frac{\rho g r^2}{\gamma} \tag{1}$$

$$\mathrm{Ca} = \frac{\mu U}{\gamma} \tag{2}$$

Where, ρ is the density of the coating fluid, g is the gravitational acceleration, r is the radius of the fluid meniscus, μ is the viscosity of the fluid, U is the speed of the linear back-and-forth motion of the coating plate, and γ is the surface tension of the fluid. In this study, a low bond number (~0.046) and a low capillary number (~0.00147) caused the cylindrical meniscus to spread between the plate and substrate, which is similar to previous process characteristics, as illustrated in coating process of Scheme 1. Considering these low dimensionless numbers, the film thickness strongly depended on the number of coatings (NC), deposition number (DN), deposition speed (DS), and CCN concentration [30, 31, 39–41]. The DS and DN were fixed at 40 mm/s and 10, respectively, for efficient alignment and coverage. A CCN concentration of 1.5 mg/mL was employed for comparison with previous reports, as the transmittance range of the CCNs was 75%–90% at different NCs (Fig. 2(b)). By controlling these parameters, uniform and efficient connected CCNs were obtained, as evidenced by OM and SEM (Figs. 2(c) and 2(d)).

3.3 Patterning process

According to the device requirements, different patterning shapes and dimensions must be produced [2, 13]. Therefore, we proposed a feasible method for

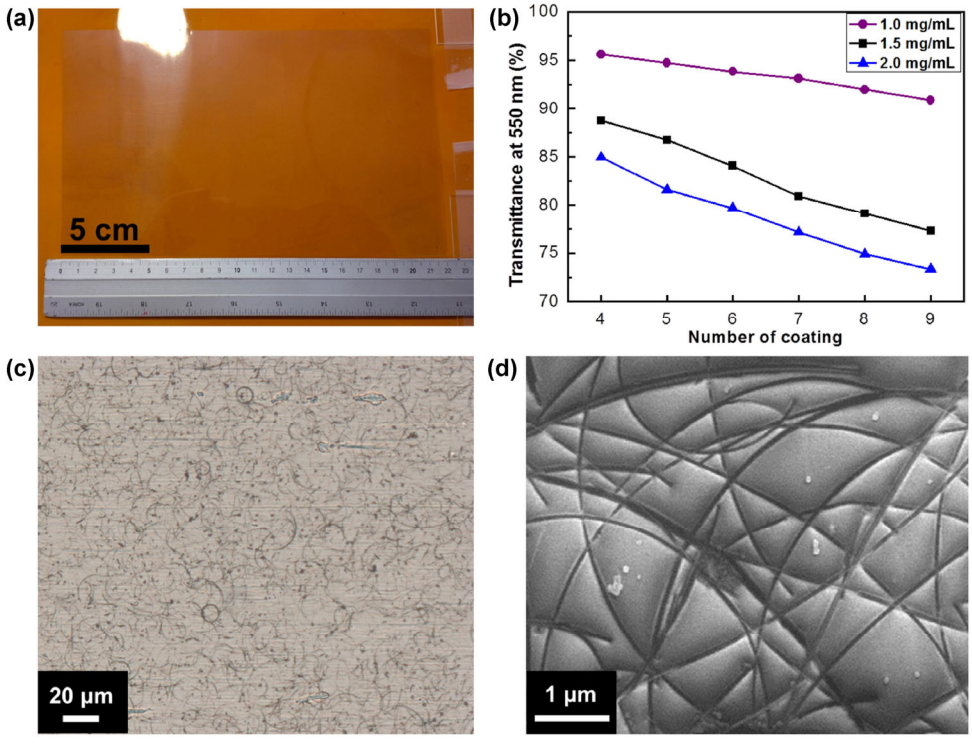

Figure 2 (a) Large-scale coating of the CCNs on the PI film. (b) Control of the transmittance according to the coating conditions in the MDD. (c) OM and (d) SEM images of uniformly coating the CCNs on the PI film.

20-μm patterning in the CCN-based FTCE fabrication (Scheme 1). The proposed PU-stamped patterning method was used to remove the contact parts of the CCNs from the PI substrate by embedding them in pre-cured PU. To fabricate the line-space pattern on the PU, urethane liquid monomers were cured at 40 ℃ on the patterned PDMS substrate. After 5 h of pre-curing, the reverse-patterned PU mold was fully formed and stamped on the CCN thin film (77.26% T of sample before washing) on the PI substrate. As a result, the unwelded NWs were embedded into the convex parts of the PU mold, forming the same line-space patterns on the CCN thin films as those on the PDMS mold.

3.4 Welding process

In addition to the random distribution, the contact resistance in the junctions is another significant factor affecting the optoelectrical performance of metal NW thin films [22, 27, 42]. The network of CCNs can be divided between percolation-type and contact-type [21, 43, 44]. Generally, thermal-sintering methods are applied under reducing-gas conditions to remove the oxide layer and improve the electrical properties via the deep percolation of NWs [21, 45]. However, vacuum facilities and harsh conditions are often needed to prevent oxidation and connect the NW junctions, which makes continuous manufacturing difficult. Washing methods involve removing the oxide layer for the direct contact of NWs through chemical reactions with the solvent [19, 46]. Unfortunately, the secondary oxidation on the junction parts caused by exposure to air degrades the electrical performance of the contact-type CCNs. Recently, light irradiation—as a photonic welding method—was reported to effectively percolate metal NWs under ambient conditions [47]. However, the pulse controllers in light-irradiation systems are unsuitable for widespread use, owing to the precise production required for the delivery of a high electrical current in milliseconds.

To overcome this critical drawback, we proposed an effective strategy of solvent-dipped welding for improving the electrical performance. The natural oxide layer on the CCN surface was removed via the

reduction reaction when the PEG_{200} was heated to 200 ℃ and maintained for 30 min (Scheme 1 and Fig. S6 in the ESM). Then, the CCN thin film was gradually conducted and exhibited the best electrical properties with the contact-type CCN connection. For a completely percolated NW connection, a low pressure of 0.3 N/cm^2 was applied for the welding of the NWs in order to reduce the contact resistance while the NWs were immersed and annealed in PEG_{200} at 200 ℃. The PEG_{200} not only protected the CCNs from oxidation during the welding process but also formed a thin liquid film between the weight and the CCNs to prevent scratches due to direct contact. SEM and HR-TEM were performed to observe the percolated CCN network after the solvent-dipped welding process. The randomly distributed and intact NW network is clearly observed in Figs. 3(a) and 3(b). During thermal treatment above 150 ℃, the surface atoms of the Cu NWs became sufficiently active to be welded [48]. Although the annealing process provided enough energy for the welding of the CCNs, the buoyancy of the solvent and the solvent layer in the junctions were critical obstacles Thus, an auxiliary pressure of 0.3 N/cm^2 was applied to reduce the force of buoyancy and minimize the gap of CCNs, similar to an Ohmic contact [49]. In this condition, the active atoms overcame the gap of the NW contact point and were connected to the metallic bonding, which was further integrated by completely crystalline Cu. The atomic arrangement of the welding parts followed the (111) planes of NW1 and NW2, which maintained their original lattice spacing and crystal orientation (Figs. 3(c) and 3(d)). However, the fringe lattice spacing on the (200) and (220) planes was stretched to 0.36 nm with the gradual rotation of the crystal orientation, because of the metallic bonding in the cross-sectional junction (Fig. 3(d)). The different live fast Fourier transform (FFT) patterns for NW1, NW2, and the welded junction, as well as a corresponding schematic image, are shown in Fig. S7 in the ESM. According to the FFT analysis, the patterns for NW1 and NW2 exhibit two typical cases of the CCNs, which are attributed to perpendicular and parallel beams on an exposed plane, respectively [8]. In addition, the welded parts exhibited new complete patterns according to the welding mechanism—not the overlapping patterns of NW1 and NW2.

After the welding was complete, the CCN thin films were washed with acetone to remove the residual PEG_{200} and unconnected NWs. This enhanced the

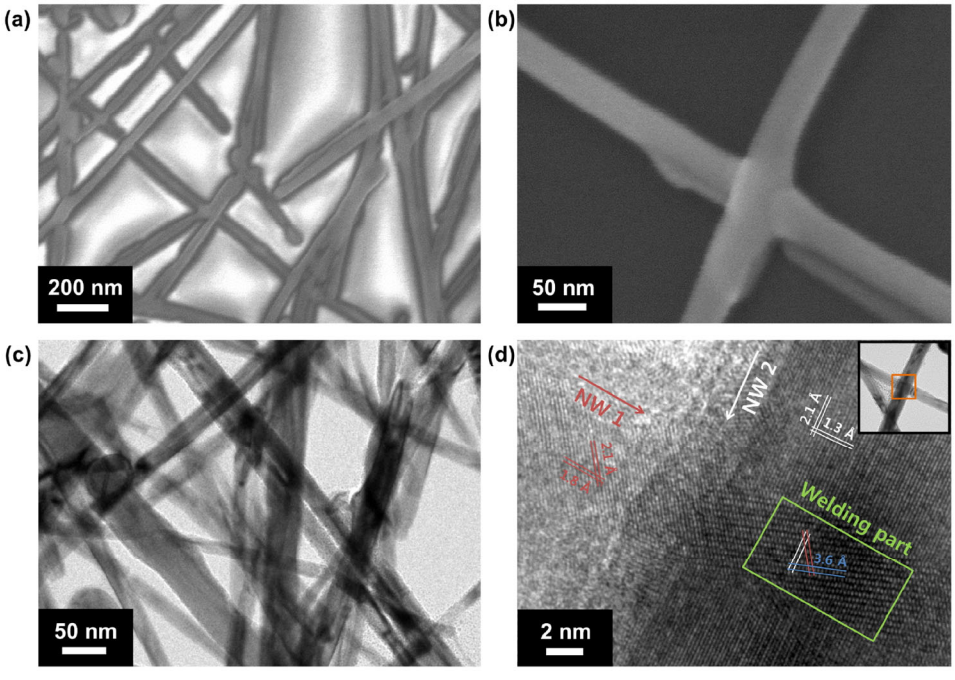

Figure 3 (a) and (b) SEM and (c) and (d) HR-TEM images of the percolated CCN network formed via the solvent-dipped welding method.

transmittance, as shown in Fig. 4(a). As previously reported, GC with a high viscosity requires considerable solvent consumption for the complete removal of the residue in the washing process. Therefore, PEG_{200}, which has a relatively low viscosity, was used for the reduction of the CCNs and better removal of the residue. The CCN thin films fabricated in this study had excellent electrical properties and a high transparency, as shown in Fig. 4(b) (R_s = 21.15 Ω/□ at 80.88% T; R_s = 35.68 Ω/□ at 82.51% T; R_s = 47.30 Ω/□ at 84.59% T; R_s = 65.72 Ω/□ at 86.80% T; R_s = 82.71 Ω/□ at 89.45% T; R_s = 132.59 Ω/□ at 91.01% T). Additionally, compared with other FTCEs, the proposed CCN thin films yielded high optoelectrical performance [13, 19, 32, 50, 51] (Fig. S8 in the ESM). We selected the 84.59% T film as a standard sample to perform systematic experiments. The solvent-dipped welding improved the oxidation stability of the CCN thin film, and Fig. 4(c) shows the relative-resistance change (R/R_0) over 10 days of exposure to air. The R/R_0 of the reduced CCN thin films without any pressure was dramatically increased to 1.17, owing to the secondary oxidation on the junctions. Compared with the reduced film, the CCNs percolated via solvent-dipped welding merged, forming a complete crystal structure with the junction gaps removed, which not only reduced the contact resistance but also prevented oxidation. Nevertheless, the R/R_0 of the welded CCN thin film was slightly increased (<5%) by the natural oxidation on the surface of the CCN films.

3.5 Transfer process

Although the CCN thin films exhibited high optoelectrical performance, the critical technical problem of the high surface roughness was unsolved for the CCNs deposited on the PI substrate. Furthermore, the PI substrate has low transparency for use in optical-device fabrication. To overcome this roughness issue, we proposed a PU-embedded transfer method, as illustrated in Scheme 1. The liquid monomers of the PU elastomer were mixed and coated on a flexible transparent substrate. After 10 h of pre-curing at 40 °C, another 30 min of pressing was applied to the PU-contacted CCN thin for a successful transfer. The

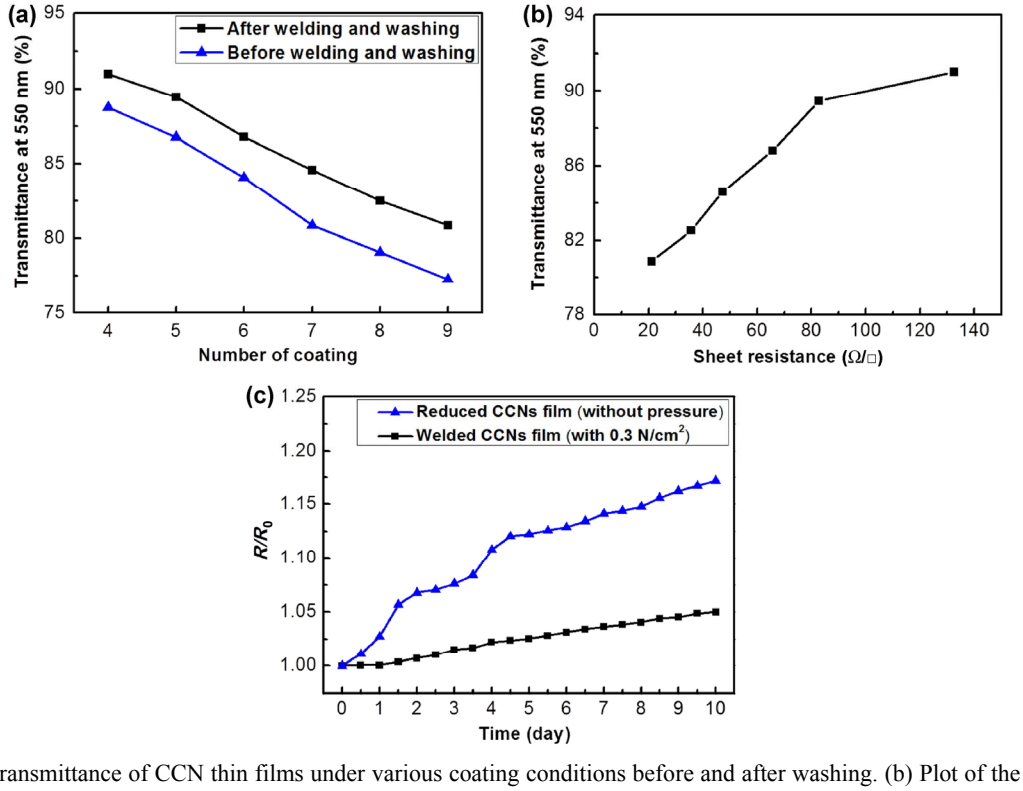

Figure 4 (a) Transmittance of CCN thin films under various coating conditions before and after washing. (b) Plot of the transmittance at 550 nm vs. the sheet resistance for CCN thin films on the PI substrate. (c) Oxidation stability of the CCN thin films before and after welding within 10 days.

PU matrix was peeled from the flexible transparent substrate when the PU was perfectly cured (Scheme 1). The transfer method involved partially embedding the CCN thin film into the pre-curing PU substrate by controlling the pre-curing time, pressure, and pressing time (Fig. 5). Therefore, the embedding depth depended on the hardness of the PU matrix, the parallel force acting in the embedding direction, and the retention time of the exerted force. Furthermore, the pre-curing PU matrix exhibited strong adhesion and a large curing force, completing the transfer of the CCNs. The aforementioned patterning process was implemented using the same method. Through the observation of R/R_0 with the adjustment of several experimental conditions, the optimal transfer conditions were determined as follows: a pre-curing time of 10 h, pressure of 0.12 N/cm^2, and pressing time of 30 min (Figs. 5(a)–5(c)). Different experimental conditions with fine-tuning yielded similar results, allowing short-time consumption and room-temperature fabrication.

3.6 FTCE

The transmittance and sheet resistance of the CCN thin film were slightly enhanced after the transfer process because several unconnected CCNs remained owing to their strong bonds with the PI substrate. Typically, the CCN thin film partially embedded into the PU matrix exhibited a low sheet resistance of 53.48 Ω/□ at a high transparency of 85.71% and a low root-mean-square surface roughness (R_{rms}) of 14.36 nm (Figs. 6(a) and 6(b)). An AFM image showing the surface topography of a CCN-based FTCE for the full data range at 15 μm × 15 μm is presented in Fig. 6(b). The highly percolated CCN network was strongly grasped by the PU matrix, enhancing the robustness. To demonstrate the high adhesion resistance, the CCN-based FTCE was stuck to adhesive tape and peeled off 10 times. As shown in the inset images of Fig. 6(c), the CCN network was not removed from the PU matrix even after being peeled from the tape 10 times. However, a small fraction of the weak NWs or partially welded junctions was unable to endure the adhesion force and broke during the repeated tape testing. Although the R/R_0 increased slightly with the successive tape tests, it remained below 1.10 at the 10th peeling repetition, indicating sufficient mechanical

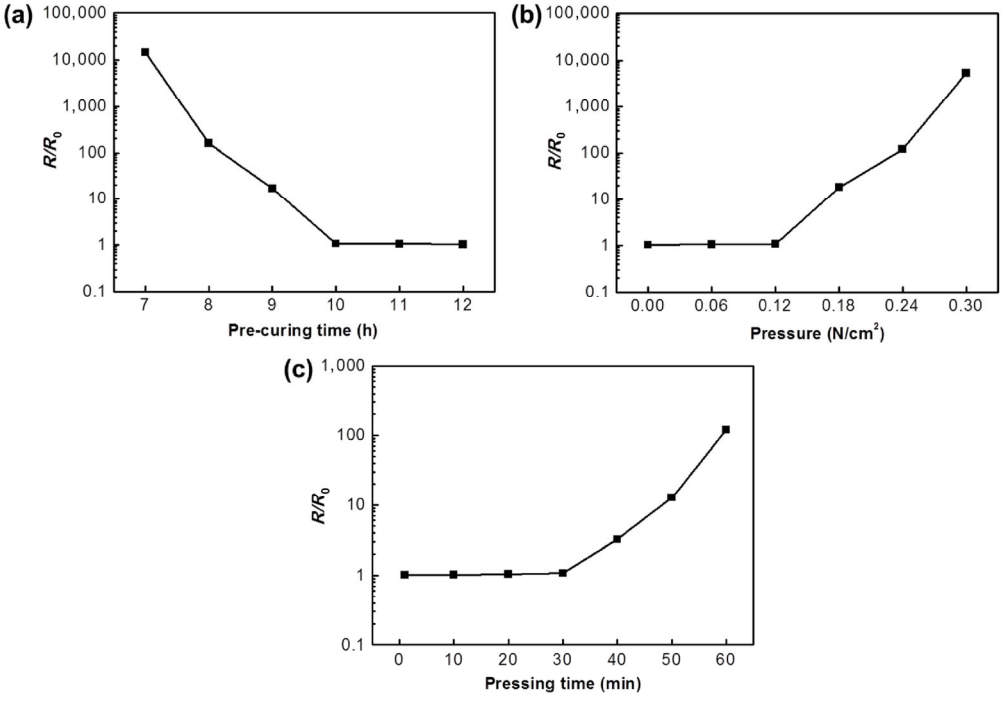

Figure 5 Relative resistance (R/R_0) of CCN thin films after transfer to the PU matrix with (a) different pre-curing times at a pressure of 0.12 N/cm^2 and a pressing time of 30 min, (b) different pressures at a pre-curing time of 10 h and a pressing time of 30 min, and (c) different pressing times at a pre-curing time of 10 h and a pressure of 0.12 N/cm^2.

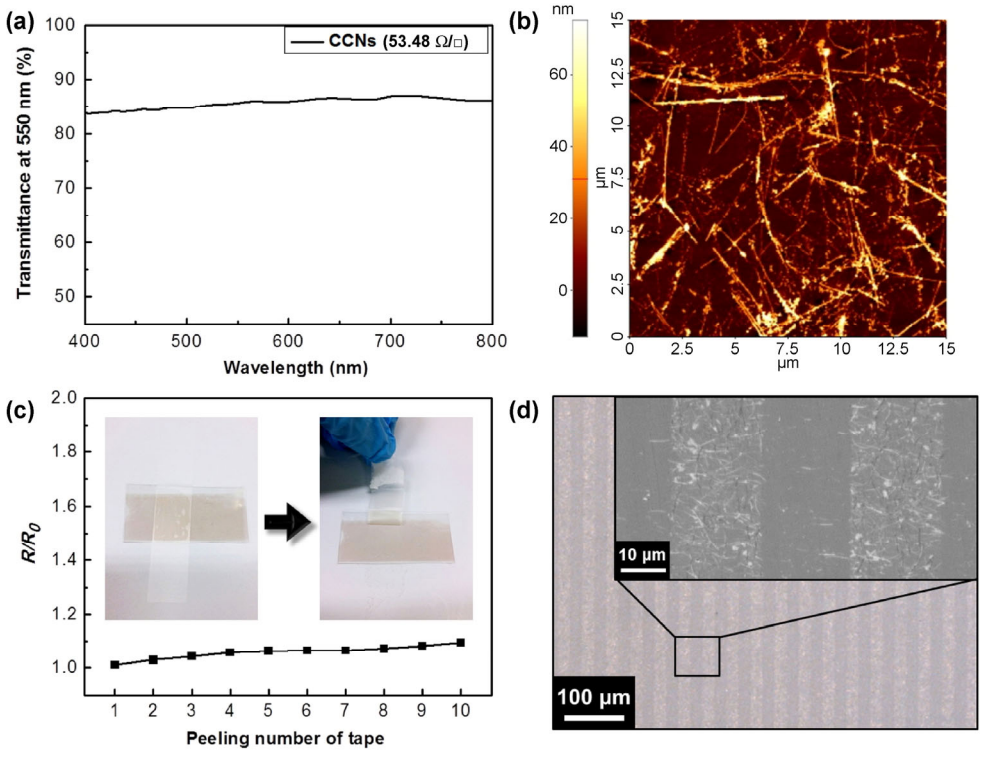

Figure 6 (a) UV–vis transmission spectrum and (b) AFM image of the CCN thin film (T = 85.71%, R_s = 53.48 Ω/□, and R_{rms} = 14.36 nm) on a PU matrix. (c) Relative resistance of the CCN thin film embedded on the PU matrix with 10 tape-peeling repetitions. (d) OM images of a 20-μm line-space patterned CCN thin film (80.88% T of the sample, after washing) embedded on a PU matrix.

stability against adhesion (Fig. 6(c)). More interestingly, this fabrication method for FTCEs was also applied to a patterned CCN thin film through the aforementioned patterning process. The OM images shown in Fig. 6(d) clearly indicate the 20-μm line-space patterned CCN network (80.88% T of sample, after washing) partially embedded into the PU substrate through the consecutive processes of synthesis, coating, patterning, welding, and transfer.

The smooth, robust, and patternable FTCE was finally completed using the all-solution method and exhibited an excellent transparency, a low sheet resistance, and high flexibility (Fig. 7(a)). To understand the relationship between the electrical performance and the flexibility, the CCNs/PU composites on the PET substrate were investigated using a self-designed bending machine. The bending-motion speed was fixed at 50 mm/s for a 5-mm bending radius and 1 to 1,000 bending cycles. Normally, the CCNs/PU composites were freestanding after being peeled from the flexible transparent substrate (Scheme 1). However, the PU was not suitable for repeated flexibility tests, because its high elastic modulus easily induced plastic deformation. Therefore, PET, which has a relatively low elastic modulus, was used as a supporting substrate to enhance the flexibility for a successful test. Figure 7(b) shows the resistance change that occurred when the CCN-based FTCE was bent with radii of 20, 15, 10, and 5 mm in the first cycle. According to previous research, CCN thin films on a PET substrates exhibit a very small resistance change under tensile or compressive bending owing to their self-bendable structure and high softness. However, in the present study, the variation in R/R_0 increased to 1.85 and 2.13 under tensile and compressive bending, respectively, with a bending radius of 5 mm. In the absence of the PU matrix that immobilized the CCNs, the free space was sufficient to release the bending strain by extending the curved shape of NWs and the random network structure of the FTCE. In contrast, when the CCN film was partially embedded into the PU matrix, the bending of the FTCE deformed the surface area of

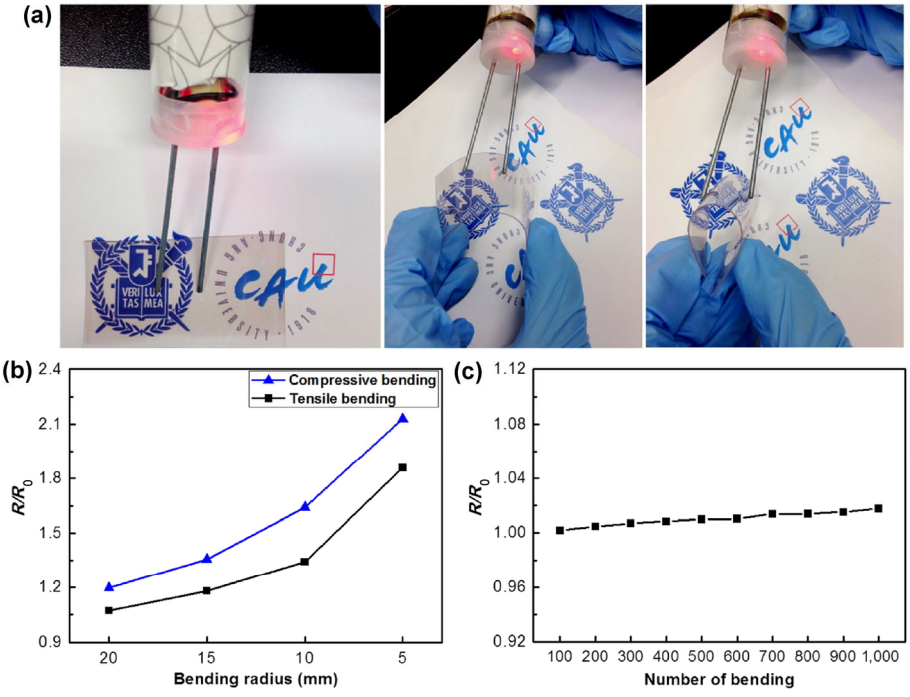

Figure 7 (a) Lighting images of a light-emitting diode connected by the CCN thin film (T = 85.71%, R_s = 53.48 Ω/□) on PU/PET with an external power supply. The relative resistance of the CCN thin film partially embedded into the PU/PET under bending with radii of (b) 20, 15, 10, and 5 mm and (c) the cycling number of the bending with a 5-mm radius.

the PU matrix with the fixed CCNs, maintaining the neutral axis of the matrix. The strain of the entire film was uniformly diffused by the stretching of the PU matrix, and it was difficult to expand the curved shape of the NWs efficiently and the random network of the electrode, resulting in a decrease of the CCN concentration and a decrease of the current density in some regions. Therefore, the R/R_0 changed significantly during the bending process, especially at a high transparency. Although the homogeneous stress induced by the PU matrix obstructed the release of the curved shape, the structural advantages of the CCNs were observed in the bending tests. As shown in Fig. 7(c), the change in R/R_0 was negligible (<1.02) after 1,000 cycles of tensile bending, indicating that the CCN-based FTCEs were highly mechanically stable against the bending.

4 Conclusions

We demonstrated a fully solution-processed approach for fabricating robust and patternable CCN-based FTCEs using self-designed innovative techniques, such as multi-polyol synthesis, MDD, PU-stamped patterning, solvent-dipped welding, and PU-embedded transfer. Furthermore, a combination of these methods solved the technical problems faced in the manufacturing of Cu NW-based FTCEs, such as the difficulty of patterning, low robustness, and high roughness. As a prospective FTCE, a uniform and highly percolated CCN thin film embedded on a PU matrix exhibited excellent optoelectrical performance (R_s = 53.48 Ω/□ at T = 85.71%) and high mechanical stability (R/R_0 < 1.02 at 1,000th bending cycle and R/R_0 < 1.10 at 10th repetition of tape peeling), along with a low surface roughness (R_{rms} = 14.36 nm). The proposed CCN-based FTCEs are applicable for many advanced flexible electronics.

Acknowledgements

This work was supported by the National Research Foundation of Korea (NRF) grant funded by the Korea government (MSIP, Ministry of Science, ICT & Future Planning) (Nos. 2016R1A2B4012992, 2016R1C1B2013145 and 2016M3A7B4910458).

Electronic Supplementary Material: Supplementary material (detailed schematic illustration of FTCEs fabrication, SEM images of Cu NWs, UV–vis spectroscopy measurement of CCNs, HR-TEM measurement of CCNs welding, comparison of other FTCEs) is available in the online version of this article at http://dx.doi.org/10.1007/s12274-017-1523-5.

References

[1] Ye, S. R.; Rathmell, A. R.; Chen, Z. F.; Stewart, I. E.; Wiley, B. J. Metal nanowire networks: The next generation of transparent conductors. *Adv. Mater.* **2014**, *26*, 6670−6687.

[2] Zhong, Z. Y.; Woo, K.; Kim, I.; Hwang, H.; Kwon, S.; Choi, Y. M.; Lee, Y.; Lee, T. M.; Kim, K.; Moon, J. Roll-to-roll-compatible, flexible, transparent electrodes based on self-nanoembedded Cu nanowires using intense pulsed light irradiation. *Nanoscale* **2016**, *8*, 8995−9003.

[3] Lee, J.; Lee, P.; Lee, H. B.; Hong, S. K.; Lee, I.; Yeo, J.; Lee, S. S.; Kim, T. S.; Lee, D. J.; Ko, S. H. Room-temperature nanosoldering of a very long metal nanowire network by conducting-polymer-assisted joining for a flexible touch-panel application. *Adv. Funct. Mater.* **2013**, *23*, 4171–4176.

[4] Mayousse, C.; Celle, C.; Carella, A.; Simonato, J.-P. Synthesis and purification of long copper nanowires. application to high performance flexible transparent electrodes with and without PEDOT:PSS. *Nano Res.* **2014**, *7*, 315−324.

[5] Li, S. J.; Chen, Y. Y.; Huang, L. J.; Pan, D. C. Large-scale synthesis of well-dispersed copper nanowires in an electric pressure cooker and their application in transparent and conductive networks. *Inorg. Chem.* **2014**, *53*, 4440–4444.

[6] Hecht, D. S.; Hu, L. B.; Irvin, G. Emerging transparent electrodes based on thin films of carbon nanotubes, graphene, and metallic nanostructures. *Adv. Mater.* **2011**, *23*, 1482–1513.

[7] Lee, J. H.; Shin, D. W.; Makotchenko, V. G.; Nazarov, A. S.; Fedorov, V. E.; Kim, Y. H.; Choi, J. Y.; Kim, J. M.; Yoo, J. B. One-step exfoliation synthesis of easily soluble graphite and transparent conducting graphene sheets. *Adv. Mater.* **2009**, *21*, 4383–4387.

[8] Zhang, W.; Yin, Z. X.; Chun, A.; Yoo, J.; Kim, Y. S.; Piao, Y. Z. Bridging oriented copper nanowire-graphene composites for solution-processable, annealing-free, and air-stable flexible electrodes. *ACS Appl. Mater. Interfaces* **2016**, *8*, 1733–1741.

[9] Robinson, J. T.; Perkins, F. K.; Snow, E. S.; Wei, Z. Q.; Sheehan, P. E. Reduced graphene oxide molecular sensors. *Nano Lett.* **2008**, *8*, 3137–3140.

[10] Pham, D. T.; Lee, T. H.; Luong, D. H.; Yao, F.; Ghosh, A.; Le, V. T.; Kim, T. H.; Li, B.; Chang, J.; Lee, Y. H. Carbon nanotube-bridged graphene 3D building blocks for ultrafast compact supercapacitors. *ACS Nano* **2015**, *9*, 2018–2027.

[11] Peng, H. J.; Huang, J. Q.; Zhao, M. Q.; Zhang, Q.; Cheng, X. B.; Liu, X. Y.; Qian, W. Z.; Wei, F. Nanoarchitectured graphene/CNT@porous carbon with extraordinary electrical conductivity and interconnected micro/mesopores for lithium-sulfur batteries. *Adv. Funct. Mater.* **2014**, *24*, 2772–2781.

[12] Kim, Y.; Ryu, T. I.; Ok, K.-H.; Kwak, M.-G.; Park, S.; Park, N.-G.; Han, C. J.; Kim, B. S.; Ko, M. J.; Son, H. J. et al. Inverted layer-by-layer fabrication of an ultraflexible and transparent Ag nanowire/conductive polymer composite electrode for use in high-performance organic solar cells. *Adv. Funct. Mater.* **2015**, *25*, 4580–4589.

[13] Han, S.; Hong, S.; Ham, J.; Yeo, J.; Lee, J.; Kang, B.; Lee, P.; Kwon, J.; Lee, S. S.; Yang, M.-Y. et al. Fast plasmonic laser nanowelding for a Cu-nanowire percolation network for flexible transparent conductors and stretchable electronics. *Adv. Mater.* **2014**, *26*, 5808–5814.

[14] Im, H.-G.; Jung, S.-H.; Jin, J.; Lee, D.; Lee, J.; Lee, D.; Lee, J.-Y.; Kim, I.-D.; Bae, B.-S. Flexible transparent conducting hybrid film using a surface-embedded copper nanowire network: A highly oxidation-resistant copper nanowire electrode for flexible optoelectronics. *ACS Nano* **2014**, *8*, 10973–10979.

[15] Hu, W. L.; Wang, R. R.; Lu, Y. F.; Pei, Q. B. An elastomeric transparent composite electrode based on copper nanowires and polyurethane. *J. Mater. Chem. C* **2014**, *2*, 1298–1305.

[16] Nam, S.; Song, M.; Kim, D.-H.; Cho, B.; Lee, H. M.; Kwon, J.-D.; Park, S.-G.; Nam, K.-S.; Jeong, Y.; Kwon, S.-H. et al. Ultrasmooth, extremely deformable and shape recoverable Ag nanowire embedded transparent electrode. *Sci. Rep.* **2014**, *4*, 4788.

[17] Rathmell, A. R.; Wiley, B. J. The synthesis and coating of long, thin copper nanowires to make flexible, transparent conducting films on plastic substrates. *Adv. Mater.* **2011**, *23*, 4798–4803.

[18] Chu, C. R.; Lee, C.; Koo, J.; Lee, H. M. Fabrication of sintering-free flexible copper nanowire/polymer composite transparent electrodes with enhanced chemical and mechanical stability. *Nano Res.* **2016**, *9*, 2162–2173.

[19] Yin, Z. X.; Song, S. K.; You, D. J.; Ko, Y.; Cho, S.; Yoo, J.; Park, S. Y.; Piao, Y. Z.; Chang, S. T.; Kim, Y. S. Novel synthesis, coating, and networking of curved copper nanowires for flexible transparent conductive electrodes. *Small* **2015**, *11*, 4576–4583.

[20] Ding, S.; Jiu, J. T.; Gao, Y.; Tian, Y. H.; Araki, T.; Sugahara, T.; Nagao, S.; Nogi, M.; Koga, H.; Suganuma, H. et al. One-step fabrication of stretchable copper nanowire

conductors by a fast photonic sintering technique and its application in wearable devices. *ACS Appl. Mater. Interfaces* **2016**, *8*, 6190–6199.

[21] Zhang, D. Q.; Wang, R. R.; Wen, M. C.; Weng, D.; Cui, X.; Sun, J.; Li, H. X.; Lu, Y. F. Synthesis of ultralong copper nanowires for high-performance transparent electrodes. *J. Am. Chem. Soc*. **2012**, *134*, 14283–14286.

[22] Yin, Z. X.; Lee, C.; Cho, S.; Yoo, J.; Piao, Y. Z.; Kim, Y. S. Facile synthesis of oxidation-resistant copper nanowires toward solution-processable, flexible, foldable, and free-standing electrodes. *Small* **2014**, *10*, 5047–5052.

[23] Guo, H. Z.; Chen, Y. Z.; Ping, H. M.; Jin, J. R.; Peng, D.-L. Facile synthesis of Cu and Cu@Cu–Ni nanocubes and nanowires in hydrophobic solution in the presence of nickel and chloride ions. *Nanoscale* **2013**, *5*, 2394–2402.

[24] Guo, H. Z.; Chen, Y. Z.; Cortie, M. B.; Liu, X.; Xie, Q. S.; Wang, X.; Peng, D.-L. Shape-selective formation of monodisperse copper nanospheres and nanocubes via disproportionation reaction route and their optical properties. *J. Phys. Chem. C* **2014**, *118*, 9801−9808.

[25] Zhan, Y. J.; Lu, Y.; Peng, C.; Lou, J. Solvothermal synthesis and mechanical characterization of single crystalline copper nanorings. *J. Cryst. Growth* **2011**, *325*, 76–80.

[26] Zhou, L.; Fu, X.-F.; Yu, L.; Zhang, X.; Yu, X.-F.; Hao, Z.-H. Crystal structure and optical properties of silver nanorings. *Appl. Phys. Lett.* **2009**, *94*, 153102.

[27] Bhanushali, S.; Ghosh, P.; Ganesh, A.; Cheng, W. L. 1D copper nanostructures: Progress, challenges and opportunities. *Small* **2015**, *11*, 1232–1252.

[28] Rathmell, A. R.; Nguyen, M.; Chi, M. F.; Wiley, B. J. Synthesis of oxidation-resistant cupronickel nanowires for transparent conducting nanowire networks. *Nano Lett.* **2012**, *12*, 3193–3199.

[29] Christensen, G.; Younes, H.; Hong, H. P.; Smith, P. Effects of solvent hydrogen bonding, viscosity, and polarity on the dispersion and alignment of nanofluids containing Fe_2O_3 nanoparticles. *J. Appl. Phys.* **2015**, *118*, 214302.

[30] Ko, Y.; Song, S. K.; Kim, N. H.; Chang, S. T. Highly transparent and stretchable conductors based on a directional arrangement of silver nanowires by a microliter-scale solution process. *Langmuir* **2016**, *32*, 366–373.

[31] Ko, Y. U.; Cho, S. R.; Choi, K. S.; Park, Y.; Kim, S. T.; Kim, N. H.; Kim, S. Y.; Chang, S. T. Microlitre scale solution processing for controlled, rapid fabrication of chemically derived graphene thin films. *J. Mater. Chem.* **2012**, *22*, 3606–3613.

[32] Hu, L. B.; Kim, H. S.; Lee, J. Y.; Peumans, P.; Cui, Y. Scalable coating and properties of transparent, flexible, silver nanowire electrodes. *ACS Nano* **2010**, *4*, 2955–2963.

[33] Kitano, T.; Maeda, Y.; Akasaka, T. Preparation of transparent and conductive thin films of carbon nanotubes using a spreading/coating technique. *Carbon* **2009**, *47*, 3559–3565.

[34] Park, S.; Pitner, G.; Giri, G.; Koo, J. H.; Park, J.; Kim, K.; Wang, H. L.; Sinclair, R.; Wong, H. S. P.; Bao, Z. Large-area assembly of densely aligned single-walled carbon nanotubes using solution shearing and their application to field-effect transistors. *Adv. Mater.* **2015**, *27*, 2656–2662.

[35] Choi, D. Y.; Kang, H. W.; Sung, H. J.; Kim, S. S. Annealing-free, flexible silver nanowire-polymer composite electrodes via a continuous two-step spray-coating method. *Nanoscale* **2013**, *5*, 977–983.

[36] Jang, E. Y.; Kang, T. J.; Im, H. W.; Kim, D. W.; Kim, Y. H. Single-walled carbon-nanotube networks on large-area glass substrate by the dip-coating method. *Small* **2008**, *4*, 2255–2261.

[37] Duan, S. K.; Niu, Q. L.; Wei, J. F.; He, J. B.; Yin, Y. A.; Zhang, Y. Water-bath assisted convective assembly of aligned silver nanowire films for transparent electrodes. *Phys. Chem. Chem. Phys.* **2015**, *17*, 8106–8112.

[38] Dai, H.; Ding, R. Q.; Li, M. C.; Huang, J.; Li, Y. F.; Trevor, M. Ordering Ag nanowire arrays by spontaneous spreading of volatile droplet on solid surface. *Sci. Rep.* **2014**, *4*, 6742.

[39] Ko, Y. U.; Kim, N. H.; Lee, N. R.; Chang, S. T. Meniscus-dragging deposition of single-walled carbon nanotubes for highly uniform, large-area, transparent conductors. *Carbon* **2014**, *77*, 964–972.

[40] Landau, L.; Levich, B. Dragging of a liquid by a moving plate. *Acta Physicochim. URSS* **1942**, *17*, 42–54.

[41] White, D. A.; Tallmadge, J. A. Theory of drag out of liquids on flat plates. *Chem. Eng. Sci.* **1965**, *20*, 33–37.

[42] Wang, R. R.; Zhai, H. T.; Wang, T.; Wang, X.; Cheng, Y.; Shi, L. J.; Sun, J. Plasma-induced nanowelding of a copper nanowire network and its application in transparent electrodes and stretchable conductors. *Nano Res.* **2016**, *9*, 2138–2148.

[43] Lim, G.-H.; Lee, N.-E.; Lim, B. Highly sensitive, tunable, and durable gold nanosheet strain sensors for human motion detection. *J. Mater. Chem. C* **2016**, *4*, 5642–5647.

[44] Lee, J.; Lee, I.; Kim, T.-S.; Lee, J.-Y. Efficient welding of silver nanowire networks without post-processing. *Small* **2013**, *9*, 2887–2894.

[45] Sachse, C.; Weiß, N.; Gaponik, N.; Müller-Meskamp, L.; Eychmüller, A.; Leo, K. ITO-free, small-molecule organic solar cells on spray-coated copper-nanowire-based transparent electrodes. *Adv. Energy Mater.* **2014**, *4*, 1300737.

[46] Won, Y.; Kim, A.; Lee, D.; Yang, W.; Woo, K.; Jeong, S.; Moon, J. Annealing-free fabrication of highly oxidation-resistive copper nanowire composite conductors for photovoltaics. *NPG Asia Mater.* **2014**, *6*, e105.

[47] Yang, H. Y.; Park, H.-W.; Kim, S. J.; Hong, J.-M.; Kim, T. W.; Kim, D. H.; Lim, J. A. Intense pulsed light induced crystallization of a liquid-crystalline polymer semiconductor for efficient production of flexible thin-film transistors. *Phys. Chem. Chem. Phys.* **2016**, *18*, 4627–4634.

[48] Guo, H. Z.; Lin, N.; Chen, Y. Z.; Wang, Z. W.; Xie, Q. S.; Zheng, T. C.; Gao, N.; Li, S. P.; Kang, J. Y.; Cai, D. J. et al. Copper nanowires as fully transparent conductive electrodes. *Sci. Rep.* **2013**, *3*, 2323.

[49] Tang, Y.; Gong, S.; Chen, Y.; Yap, L. W.; Cheng, W. L. Manufacturable conducting rubber ambers and stretchable conductors from copper nanowire aerogel monoliths. *ACS Nano* **2014**, *8*, 5707–5714.

[50] Rathmell, A. R.; Bergin, S. M.; Hua, Y.-L.; Li, Z.-Y.; Wiley, B. J. The growth mechanism of copper nanowires and their properties in flexible, transparent conducting films. *Adv. Mater.* **2010**, *22*, 3558–3563.

[51] Kim, U. J.; Lee, I. H.; Bae, J. J.; Lee, S.; Han, G. H.; Chae, S. J.; Güneş, F.; Choi, J. H.; Baik, C. W.; Kim, S. et al. Graphene/carbon nanotube hybrid-based transparent 2D optical Array. *Adv. Mater.* **2011**, *23*, 3809–3814.